Title

Wide-Field Optical Coherence Tomography Imaging Improves Rate of Change Detection in Progressing Glaucomatous Eyes Compared With Standard-Field Imaging

Journal

Investigative Ophthalmology & Visual Science, 65(8)

ISSN

0146-0404

Authors

Bowd, Christopher

Belghith, Akram

Rezapour, Jasmin

et al.

Publication Date

2024-07-09

DOI

10.1167/iovs.65.8.18

Peer reviewed

Wide-Field Optical Coherence Tomography Imaging Improves Rate of Change Detection in Progressing Glaucomatous Eyes Compared With Standard-Field Imaging

Christopher Bowd,[1] Akram Belghith,[1] Jasmin Rezapour,[2] Jost B. Jonas,[3] Leslie Hyman,[4] Robert N. Weinreb,[1] and Linda M. Zangwill[1]

[1]Hamilton Glaucoma Center, Shiley Eye Institute, The Viterbi Family Department of Ophthalmology, University of California San Diego, La Jolla, California, United States
[2]Department of Ophthalmology, University Medical Center Mainz, Mainz, Germany
[3]Institute of Molecular and Clinical Ophthalmology IOB Basel, Switzerland
[4]Wills Eye Hospital, Thomas Jefferson University, Philadelphia, Pennsylvania, United States

Correspondence: Linda M. Zangwill, Hamilton Glaucoma Center, Shiley Eye Institute, The Viterbi Family Department of Ophthalmology, University of California San Diego, La Jolla, CA 92093, USA; lzangwill@health.ucsd.edu.

Received: October 31, 2023
Accepted: June 11, 2024
Published: July 9, 2024

Citation: Bowd C, Belghith A, Rezapour J, et al. Wide-field optical coherence tomography imaging improves rate of change detection in progressing glaucomatous eyes compared with standard-field imaging. *Invest Ophthalmol Vis Sci.* 2024;65(8):18. https://doi.org/10.1167/iovs.65.8.18

Purpose. To compare rates of retinal nerve fiber layer change over time in healthy, eyes with nonprogressing glaucoma and eyes with progressing glaucoma using single wide-field (SWF) and optic nerve head (ONH) cube scan optical coherence tomography (OCT) images.

Methods. Forty-five eyes of 25 healthy individuals and 263 eyes of 161 glaucoma patients from the Diagnostic Innovations in Glaucoma Study were included. All eyes underwent 24-2 visual field testing and OCT (Spectralis SD-OCT) ONH and macular imaging. SWF images (up to 43° × 28°) were created by stitching together ONH cube scans centered on the optic disc and macular cube scans centered on the fovea. Visual field progression was defined as guided progression analysis likely progression and/or a significant ($P < 0.01$) mean deviation slope of less than −1.0 dB/year. Mixed effects models were used to compare rates of change. Highly myopic eyes were included.

Results. Thirty glaucomatous eyes were classified as progressing. In eyes with glaucoma, mean global rate of change was −1.22 µm/year ($P < 0.001$) using SWF images and −0.83 µm/year ($P = 0.003$) using ONH cube scans. Rate of change was significantly greater in eyes with progressing glaucoma compared with eyes with nonprogressing glaucoma (−1.51 µm/year vs. −1.24 µm/year; $P = 0.002$) using SWF images and was similar using ONH cube scans ($P = 0.27$).

Conclusions. In this cohort that includes eyes with and without high axial myopia, the mean rate of retinal nerve fiber layer thinning measured using SWF images was faster in eyes with progressing glaucoma than in eyes with nonprogressing glaucoma. Wide-field OCT images including the ONH and macula can be effective for monitoring glaucomatous progression in patients with and without high myopia.

Keywords: glaucoma, OCT, wide-field imaging, progression, myopia

The primary goal of glaucoma treatment is to conserve visual function of the glaucoma patient, including vision-related quality of life, by stopping or slowing the progression of the disease once identified. Historically, treatment often was initiated and adjusted based on visual field (VF) testing results and assessment of the appearance of the optic disc and surrounding retina by visual examination or fundus photograph assessment. In recent decades, the assessment of optical imaging technology results have been used more frequently in areas where these technologies are available.

Evidence has indicated that combining single-modal models (i.e., models using a single measurement technique) into hybrid models can improve accuracy for detecting POAG.[1–10] Recently, we showed that combining optical coherence tomography (OCT)-based retinal nerve fiber layer (RNFL) thickness maps with texture-based en face images[11] that included optic nerve head (ONH) and partial macular regions using a deep learning classifier showed better ability to discriminate between healthy and POAG eyes than deep learning analyses of ONH thickness maps alone, particularly in high axial myopic eyes.[12]

Recent studies have indicated specifically that wide-field OCT imaging that includes both the macula and ONH is as good as or better than standard-field OCT imaging for detecting glaucoma.[13,14] The goal of the current study was to investigate the hypothesis that increasing imaging field of view size also would improve glaucoma progression

detection in eyes with and without high axial myopia. To address this hypothesis, we constructed single wide-field (SWF) en face OCT images by combining ONH and macular cube scans to determine if rates of RNFL change over time in healthy, nonprogressing glaucoma and eyes with progressing glaucoma differed between ONH thickness measurements acquired from SWF and ONH cube scans. Emmetropic, myopic and highly myopic eyes were included. The inclusion of highly myopic eyes was used to show the generalizability of results to eyes of all axial lengths.

Materials and Methods

For the current analysis, 308 eyes from 186 individuals who participated in the UC San Diego Diagnostic Innovations in Glaucoma Study (DIGS) were included. The DIGS is a longitudinal, observational study that aims to assess visual function and optic nerve structure in glaucoma, using the same protocol as the African Descent and Glaucoma Evaluation Study based at the University of California (UC) at San Diego.[15] Participants were enrolled based on the criteria specified below and all methodology was approved by the UC San Diego Human Research Protection Program/Institutional Review Board and adhered to the Declaration of Helsinki and Health Insurance Portability and Accountability Act guidelines for research involving human subjects including obtaining written informed consent for study participation. The DIGS was registered at http://cilincaltrials.gov (NCT00221897) on September 14, 2005.[15]

Participants

Study participants were 18 years of age or older and had open anterior chamber angles at study entry. All participants underwent an extensive ophthalmologic examination, including assessment of best-corrected visual acuity, slit-lamp biomicroscopy, IOP measurement with Goldmann applanation tonometry, gonioscopy, central corneal thickness measured with ultrasound pachymetry (DGH Technology, Inc, Exton, PA, USA), dilated fundus examination, simultaneous stereophotography of the optic disc, VF testing (Humphrey Field Analyzer; 24-2 Swedish Interactive Threshold Algorithm standard; Carl Zeiss Meditec, Jena, Germany), coherence interferometry measurement of the axial length (IOLMaster, Carl Zeiss Meditec, Dublin, CA, USA), and Spectralis OCT imaging (version 6.10; Heidelberg Engineering Inc, Heidelberg, Germany). Participants were excluded if they had a history of ocular surgery, except for uncomplicated glaucoma or cataract surgery ocular, or any systemic diseases that could affect the VF or optic nerve including peripapillary staphylomas.

All VFs were evaluated by UC San Diego Visual Field Assessment Center (VisFACT) personnel based on a standardized protocol.[15] Only repeatable and reliable VF tests (≤33% fixation losses and false-negative results and ≤33% false-positive results) were included and VFs with a glaucoma hemifield test (GHT) classification of abnormally high sensitivity were deemed unreliable and were excluded. Only three of the study eyes had greater than 25% fixation losses or false-positive responses.

Individual eyes were classified either POAG or healthy. POAG eyes (n = 263 eyes of 161 individuals) were classified based on the DIGS conventional standard of repeatable glaucomatous VF loss (pattern standard deviation <95% confidence limits or a GHT outside of normal limits) and corresponding optic disc or parapapillary damage based on visual inspection.[15] Stereo photograph-based glaucomatous damage was defined as focal or diffuse narrowing of the neuroretinal rim, and/or detection of RNFL defects characteristic of glaucoma based on a masked assessment by two trained observers.

To identify glaucoma in highly myopic eyes, two experts (C.B. and J.R.) graded photographs after high myopia optic disc grading training with a senior consultant (J.B.J.) with expertise in myopia and glaucoma. Stereo photograph-based optic disc damage in apparently myopic eyes was defined by consensus between both graders. In cases of disagreement, diagnosis was defined by adjudication by the senior consultant. We did not consider VF results when defining myopia. It should be noted that myopic eyes with glaucoma were selected from patients being treated for glaucoma in our clinic by glaucoma specialists.

Participants were considered healthy (n = 45 eyes of 25 individuals) if they had an IOP of 21 mm Hg or less with no history of an elevated IOP, normal-appearing optic discs, intact neuroretinal rims and peripapillary RNFLs, and a minimum of two reliable and normal VFs with pattern standard deviation within the 95% confidence limits and a GHT result within normal limits OU. Normal VFs had a mean deviation (MD) and pattern standard deviation with a P value of greater than 0.05 and a GHT result within normal limits.

The dataset included data from eyes with and without high axial myopia defined as axial length of greater than 26.0 mm as described elsewhere in this article. At least three OCT and at least four VF results (two baseline and at least two follow-up tests) with a minimum of 1.3 years of follow-up were required for participant eligibility. Data are available from the corresponding author upon reasonable request.

High Axial Length Myopia Definition

We defined high axial myopia by an axial length of more than 26.0 mm because axial elongation can lead to morphologic changes of the optic disc and the fundus[16]; myopia defined by refractive error does not necessarily reflect these changes. Moreover, cataract surgery or refractive procedures can result in a refractive shift in eyes that are axially elongated but no longer classified as (highly) myopic by refractive error.

OCT

The Spectralis OCT2 (HEYEX version 6.10; Heidelberg Engineering GmbH) was used for OCT imaging. This instrument uses an 870-nm central wavelength at an 85-kHz A-scan rate. We used a custom wide ONH cube scan of 30° × 25° (8.7 × 7.3 mm) centered on the optic disc composed of 121 horizontal B-scans and a macula cube of 30° × 25° (8.7 × 7.3 mm) centered on the fovea formed by 121 horizontal B-scans. The interval between the B-scans was 60 µm and the lateral resolution was 5.64 µm/pixel; the axial resolution was 3.87 µm/pixel, and the frame rate was 10 per B-scan. Quality review of Spectralis images required a signal strength of greater than 15 dB and were deemed acceptable quality for use based on standardized assessment by the Imaging Data Evaluation and Analysis Reading Center.

Investigative Ophthalmology & Visual Science

Generating SWF Images

Large SWF images encompassing the macula and disc were generated from the individual ONH and macula cube scans using a pyramid-based approach.[17] Specifically, to construct the SWF images vessels in the scanning laser ophthalmoscopy images for the optic disc and macula were used to generate point pairs indicating the transposition of several points in the ONH image to the macula image. The maximum SWF images was 43° × 28°, whereas ONH and macula cube scans are 30° × 25°.

There may be small differences in the exact pixels included in the RNFL thickness measurements in our stitched SWF images compared with the native wide-field scans available on some OCT instruments. It is important to note that the current SWF image is created solely on the baseline scanning laser ophthalmoscopy images, and this transformation is applied consistently to all follow-up images. The built-in registration software in the Spectralis ensures that each follow-up image is aligned with the baseline. Therefore, it is unlikely that the current montaged scans are introducing much if any additional variability to the measurements compared with the native wide-field scans available.

Retinal Layer Segmentation

Raw three-dimensional ONH and macula wide volume scans were exported to a numerical computing language (MATLAB; MathWorks, Natick, MA, USA). The San Diego Automated Layer Segmentation Algorithm (SALSA)-deep was used to automatically segment the inner limiting membrane and RNFL to define global and regional RNFL thicknesses on the ONH cube scans and SWF scans. In the current study, we used two modified grids to evaluate the longitudinal changes in RNFL thickness. Unlike the traditional ETDRS grid, which is centered on the ONH and segmented by three concentric circles (0.5, 3.0, and 6.0 mm) and divided into four sectors (temporal, superior, nasal, and inferior), our approach involved calculating the average thickness of all pixels within a circular band ranging from 3 to 7 mm diameter around the ONH center for the ONH cube and from 3 to 9 mm diameter for the SWF. Any missing segmentations resulted in the exclusion of those pixels from the calculated average. Figure shows (A) the stitched scanning laser ophthalmoscopy image, (B) the wide-field RNFL thickness map with the 3- to 9-mm measurement band superimposed, and (C) the ONH cube scan RNFL thickness map with both the 3- to 7-mm and the 3- to 9-mm measurement bands superimposed for comparison. As can be seen, the 3- to 9-mm band provides a larger area of coverage temporally and inferiorly when superimposed on the SWF image compared with superimposing the 3- to 9-mm band on the ONH cube scan (mean average additional pixels 8.3% [95 confidence interval (CI), 5.1%–10.2%]). Additionally, on average, the 3- to 9-mm band contains 26.4% more pixels compared with the 3- to 7-mm band when superimposed on the SWF RNFL thickness map. SALSA-deep segmentation accuracy of all images was subjectively assessed by co-author A.B. to exclude segmentation artifacts. No eyes were excluded from the analysis based on segmentation failure.

Definition of Progression

An eye was defined as progressing if it was identified as likely progression by VF-guided progression analysis and/or had a significant ($P < 0.01$) negative VF MD slope of less than −1.0 dB/year.[18]

Statistical Analyses

Descriptive statistics were used to compare demographic characteristics by group (healthy, glaucoma suspect and glaucoma study participants). We used χ^2 to compare categorical variables and t tests to compare continuous variables. Mixed effects models were used to calculate the estimated rates of change (slopes) for RNFL loss from baseline. Models included group (healthy vs. glaucoma, progressing eyes vs. nonprogressing eyes), time, and the interaction term Group × Time. The models were adjusted for age, mean IOP during follow-up, axial length, and Bruch's membrane opening area.

Statistical analyses were performed using Stata 14.2 (StataCorp LLC, College Station, TX, USA). P values of 0.05 or less were considered statistically significant.

Results

A total of 308 eyes from 186 individuals were included, with a mean age of 70.95 years (95% CI, 69.17–72.73 years). A total of 96 patients (52%) were female. There were 108 Caucasians (58%), 40 African Americans (21.5%), 31 Asians (16.6%), and 6 others (3%). Average follow-up time was

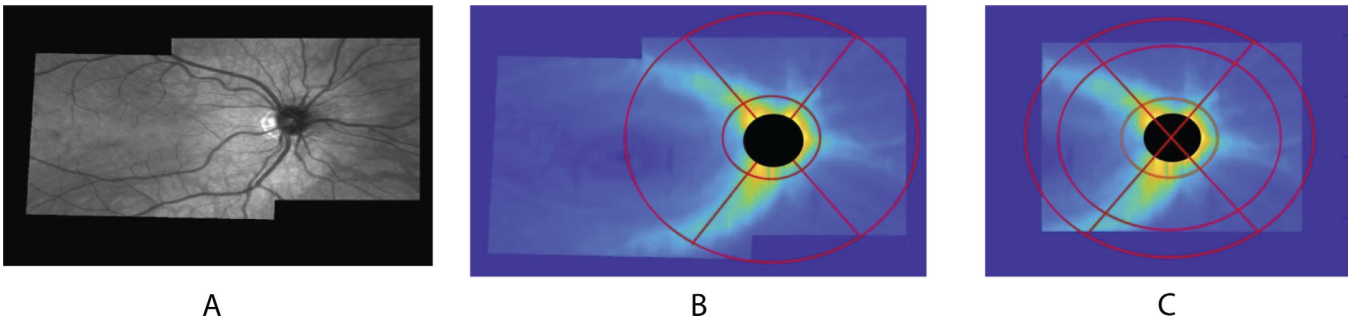

Figure. (**A**) The stitched wide-field scanning laser ophthalmoscopy image created from individual ONH and macula cube scans, (**B**) the wide-field RNFL thickness map with the 3- to 9-mm measurement band superimposed, and (**C**) the ONH cube scan RNFL thickness map with both the 3- to 7-mm measurement band and the 3- to 9-mm measurement band superimposed.

Investigative Ophthalmology & Visual Science

Table 1. Patient and Eye Characteristics by Diagnosis

	Diagnosis		
	Healthy (n = 25, 45 Eyes)	**Glaucoma (n = 161, 263 Eyes)**	***P* Value**
Age, years	62.3 (56.4 to 68.2)	72.3 (70.5 to 74.1)	<0.001
Female sex	60.0	50.1	0.01
High myopia eyes	51.0	17.0	<0.01
Progressing eyes		10.2	
Race			
Non-White	60.0	40.0	0.001
White	40.0	60.0	
MD, dB	−0.64 (−1.18 to 0.09)	−5.20 (−5.92 to −4.48)	<0.001
Follow-up, mo	28.1 (27.0 to 29.3)	30.3 (29.12 to 32.1)	0.14
IOP, mm Hg	14.95 (13.2 to 16.3)	14.09 (13.9 to 15.4)	0.57
AL, mm	25.2 (24.2 to 25.7)	24.9 (24.1 to 25.3)	0.42
Spherical equivalent, D	−5.20 (−5.91 to −4.2)	−1.54 (−1.81 to −1.41)	0.02
History of cataract surgery	12.1	47.4	<0.001
Cataract surgery during follow-up	6.66	5.7	0.09
History of glaucoma surgery	0	54	<0.001
OCT image quality signal-to-noise ratio, dB	28.12 (26.12 to 31.11)	27.33 (25.44 to 30.83)	0.38

AL, axial length.

Values are mean (95% CIs) or percent. Statistical significance of differences in continuous and categorical variables are determined by two-sample t tests and Fisher's exact test for patient level variables (respectively) and linear mixed effects models for eye-level variables.

Table 2. RNFL Thickness of ONH Cube Scan Derived and SWF-Derived Sectoral Measurements From Eyes With No Cataract Surgery During Follow-Up (42 Healthy Eyes of 25 Subjects and 248 Eyes With Glaucoma of 148 Patients)

	RNFL Thickness at Baseline, µm		
	Healthy	**Glaucoma**	***P* Value (Healthy vs. Glaucoma)**
ONH cube scan-derived RNFL			
Temporal	61.43 (58.17–63.82)	47.38 (45.74–50.12)	<0.001
Superior	72.08 (67.11–77.21)	56.35 (54.74–58.04)	<0.001
Nasal	48.66 (46.42–51.55)	44.28 (41.86–49.21)	0.34
Inferior	59.34 (58.33 62.19)	53.21 (51.93–55.43)	<0.001
Global	61.56 (57.94–61.77)	49.54 (47.65–52.54)	<0.001
SWF-derived RNFL			
Temporal	51.43 (49.67–54.09)	40.43 (39.67–42.91)	<0.001
Superior	56.32 (54.54–57.98)	50.21 (48.19–51.56)	<0.001
Nasal	43.11 (38.54–44.56)	42.67 (41.98–44.18)	0.45
Inferior	57.49 (54.41–60.62)	50.34 (48.56–52.76)	<0.001
Global	53.39 (51.94–57.47)	44–34 (43.89,49.50)	<0.001

Values are mean (95% CIs).

28.1 months for healthy eyes and 30.3 months for glaucomatous eyes. Table 1 shows baseline demographic and clinical characteristics based on the classification at entry study entry. The mean age in the healthy group was significantly younger (62.3 years [95% CI, 56.4–68.2 years]) compared with the glaucoma group (72.3 years [95% CI, 70.5–74.1 years]) ($P < 0.001$). The glaucoma group had worse VF MD ($P < 0.001$) than healthy eyes. The proportion of individuals of European descent was lower in the healthy group (40%) compared with the glaucoma group (60%) ($P = 0.001$). There was no significant difference in axial length ($P = 0.41$) and IOP ($P = 0.57$) between groups. The mean spherical equivalent was significantly lower in healthy eyes (−5.20 [95% CI, −5.91 to −4.2]) compared with eyes with glaucoma (−1.54 [95% CI, −1.81 to−1.41]), likely owing in part to the higher prevalence of a prestudy history of cataract surgery in the glaucoma group (47.4%) compared with the healthy group (12.1%). No significant difference in image quality was observed between images from healthy and glaucomatous eyes (26.11 dB and 27.33 dB, respectively; $P = 0.38$).

Three healthy eyes (6.7%) and 15 eyes with glaucoma (5.7%) underwent cataract surgery during study follow-up. These eyes were excluded from the estimate of rate of change analyses to avoid possible mischaracterization of RNFL thickening that could be attributable to improved image quality.

Baseline sectoral RNFL thickness measurements derived from the ONH cube scans and SWF images in healthy and eyes with glaucoma are presented in Table 2. Healthy eyes had thicker mean baseline RNFL in all sectors ($P < 0.001$), except the nasal sector in both ONH cube scans and SWF images (both comparisons $P \geq 0.34$).

During follow-up, 32 of 263 eyes with glaucoma (12.2%) showed progression. Among these 32 progressing eyes, 7 showed progression by VF-guided progression analysis only, 10 showed progression by VF-guided progression analysis and a significant ($P < 0.01$) slope (MD of <−1.0 dB/year), 15 showed progression by a significant ($P < 0.01$) slope (MD of <−1.0 dB/year). The average follow-up time was 27.2 months for nonprogressing eyes and 30.1 months for

Investigative Ophthalmology & Visual Science

Table 3. Patient and Eye Characteristics by Glaucoma VF Progression

	Glaucoma VF Progression Status		
	Nonprogressing Eyes (n = 147, 230 Eyes)	**Progressing Eyes (n = 27, 32 Eyes)**	***P* Value**
Age, y	71.2 (70.9 to 73.2)	70.5 (65.33 to 75.30)	0.31
Female sex	50.2	42.0	0.03
High myopia	17.8	18.75	0.45
Race			
Non-White	32.6	40.6	0.39
White	67.4	59.4	
Baseline MD, dB	−4.73 (−5.47 to −4.35)	−6.02 (−7.13 to −5.02)	0.04
Follow-up, mo	27.2 (28.7 to 31.5)	30.2 (28.6 to 32.1)	0.58
Median No. of OCT visits	5	5	0.64
Median No. of VF visits	6	6	0.47
Baseline IOP, mm Hg	14.45 (12.98 to 14.11)	14.51 (11.88 to 16.14)	0.32
AL, mm	24.43 (24.34 to 25.95)	24.74 (24.11 to 25.38)	0.67
Spherical equivalent, D	−1.54 (−1.95 to −1.28)	−0.80 (−1.88 to −0.43)	0.22
History of cataract surgery	0.47	46.87	0.61
Cataract surgery during follow-up	5.6	6.25	0.49
History of glaucoma surgery	53.47	56.25	0.39
Glaucoma surgery during follow-up	4.3	3.1	0.19

AL, axial length.

Values are mean (95% CIs) or percent. Statistical significance of differences in continuous and categorical variables are determined by two-sample *t* tests and Fisher's exact test for patient-level variables (respectively) and linear mixed effects models for eye-level variables.

Table 4. Baseline RNFL Thickness of ONH Cube Scan-Derived and SWF-Derived Sectoral Measurements From Eyes With No Cataract Surgery During Follow-Up (217 NonProgressing Eyes of 139 Patients and 30 Progressing Eyes of 26 Patients)

	RNFL Thickness at Baseline, µm		
	Nonprogressing Eyes	**Progressing Eyes**	***P* Value**
ONH cube scan-derived RNFL			
Temporal	48.45 (46.12 to 52.19)	41.11 (32.82 to 44.03)	0.02
Superior	56.43 (54.43 to 59.08)	57.32 (51.01 to 62.22)	0.41
Nasal	44.34 (41.12 to 43.56)	40.30 (32.19 to 42.03)	0.52
Inferior	53.43 (51.54 to 57.97)	54.72 (48.04 to 61.12)	0.47
Global	51.44 (48.15 to 50.17)	46.84 (42.73 to 48.24)	0.06
SWF-derived RNFL			
Temporal	41.33 (40.18 to 44.02)	36.31 (34.32 40.94)	0.01
Superior	48.45 (47.34 to 49.34)	45.82 (44.10 to 48.01)	0.02
Nasal	41.34 (39.12 to 42.44)	40.85 (36.35 to 45.09)	0.21
Inferior	50.23 (50.09 to 51.44)	51.30 (47.31 to 56.04)	0.59
Global	45.43 (44.11 to 46.96)	42.12 (38.21 to 41.31)	0.002

progressing eyes. Table 3 shows the baseline demographic and clinical characteristics for both groups. The eyes with progressing glaucoma had a worse baseline VF mean MD ($P = 0.04$) than eyes with nonprogressing glaucoma. The proportion of individuals of European descent was similar in both groups ($P = 0.39$). There were no significant differences in axial length ($P = 0.67$), baseline IOP ($P = 0.32$), or spherical equivalent ($P = 0.21$) between the groups. During follow-up, 2 eyes from the glaucoma progressing group and 13 eyes from the nonglaucoma progressing glaucoma group underwent cataract surgery. These eyes were excluded from the longitudinal analysis, resulting in 30 progressing eyes included in the progression analysis. Baseline sectoral RNFL thickness measurements derived from the ONH cube scans and SWF images in eyes with progressing glaucoma and eyes with nonprogressing glaucoma are presented in Table 4. Using ONH cube scans, the eyes with nonprogressing glaucoma had a statistically thicker baseline RNFL in the temporal sector only ($P = 0.02$), whereas using SWF images, the eyes with nonprogressing glaucoma had a statistically thicker baseline RNFL in globally and in the temporal and superior sectors (all $P < 0.002$), but not in the nasal and inferior sectors (both comparisons $P \geq 0.21$).

Estimated rates of change of global and sectoral RNFL in healthy and all eyes with glaucoma adjusted for age, mean IOP during follow-up, axial length, and Bruch's membrane opening area are presented in Table 5. A significant decrease over time (i.e., a slope with $P < 0.05$) in RNFL thickness using SWF images was observed in healthy eyes globally (−0.48 µm/year [95% CI, −0.94 to −0.23]) in the temporal sector (−0.143 µm/year [95% CI, −0.53 to−0.12]), in the superior sector (−0.23 µm/year [95% CI, −0.38 to−0.09]), and in the inferior sector (−0.59 µm/year [95% CI, −0.89 to−0.21]), whereas significant change in healthy eyes was observed globally (−0.03 µm/year [95% CI to −0.32, −0.01]) using ONH cube scans, indicating greater sensitivity to change with increased OCT sampling area. In almost all cases, using both ONH cube scans and SWF images, a

Investigative Ophthalmology & Visual Science

Table 5. RNFL Thickness of ONH Cube Scan-derived and SWF-Derived Sectoral Rate of Change From Eyes With No Cataract Surgery During Follow-up (42 Healthy Eyes of 24 Subjects and 248 Eyes With Glaucoma of 148 Patients)

	RNFL Rate of Change, µm/y		
	Healthy Eyes	Eyes With Glaucoma	*P* Value
ONH cube scan-derived RNFL			
Temporal	−0.07 (−0.31 to 0.03)	−0.55* (−0.74 to −0.42)	0.001
Superior	0.09 (−0.32 to 0.41)	−0.42* (−0.93 to −0.45)	0.003
Nasal	0.31 (−0.29 to 0.43)	−0.12 (−0.57 to 0.32)	0.29
Inferior	−0.32 (−1.03 to 0.43)	−1.32* (−1.41 to −1.09)	<0.001
Global	−0.03* (−.32 to −0.01)	−0.83* (−.97 to −0.68)	<0.001
SWF-derived RNFL			
Temporal	−0.14* (−0.53 to −0.12)	−0.81* (−1.00 to 04 to −0.87)	0.001
Superior	−0.23* (−0.38–0.09)	−1.42* (−1.53 to −1.32)	<0.001
Nasal	−0.19 (−0.43 to 0.15)	−0.21 (−0.68 to 0.45)	0.43
Inferior	−0.59* (−0.89 to −0.21)	−1.34* (−1.43–0.92)	0.004
Global	−0.48* (−0.94–0.23)	−1.22* (−1.20 to −1.10)	<0.001

* Significant slope ($P < 0.05$).

Table 6. RNFL Thickness of ONH Cube Scan-derived and SWF-derived Sectoral Rate of Change From Eyes With No Cataract Surgery During Follow-up (217 Nonprogressing Eyes of 139 Patients and 30 Progressing Eyes of 27 Patients)

	RNFL Rate of Change, µm/y		
	NonProgressing Eyes	Progressing Eyes	*P* Value
ONH cube scan-derived RNFL			
Temporal	−0.48* (−0.73 to −0.43)	−0.58* (−0.77 to −0.32)	0.42
Superior	−0.43* (−0.94 to −0.39)	−0.46* (−0.82 to −0.37)	0.22
Nasal	0.05 (−0.32 to 0.19)	−0.01 (−0.12 to 0.34)	0.47
Inferior	−1.07* (−1.31 to −1.05)	−1.18* (−1.41 to −1.09)	0.50
Global	−0.83 (−0.98 to −0.69)	−1.14* (− 1.35 to −0.53)	0.27
SWF-derived RNFL			
Temporal	−0.89* (−0.94 to −0.74)	−0.90* (−1.26 to −0.84)	0.22
Superior	−1.38* (−1.45 to −1.20)	−1.40* (−1.51 to −1.35)	0.15
Nasal	−0.24 (−0.40 to 0.09)	−0.25 (−0.42 to 0.19)	0.41
Inferior	−1.10* (−1.24 to −1.04)	−1.41* (−1.56 to −1.34)	0.01
Global	−1.24* (−1.34 to −1.07)	−1.51* (−1.82 to −1.43)	0.002

* Significant slope ($P < 0.05$).

greater decrease in RNFL thickness was observed in eyes with glaucoma than in healthy eyes, as expected (except in the nasal sector where $P \geq 0.43$). These results confirm that although some age-related RNFL thinning occurs in healthy eyes over time, a greater disease-related change occurs in POAG eyes whether they are progressing using our definition of progression or not.

Table 6 shows rate of change in global and sectoral RNFL thickness in nonprogressing and eyes with progressing glaucoma. The model shows a significant decrease in global, temporal sector, superior sector, and inferior sector measurements over time in both progressing and nonprogressing eyes. However, the rate of decline was only significantly higher in progressing eyes compared with nonprogressing eyes when SWF measurements were considered. Significant differences were observed globally (−1.51 µm/year [95% CI, −1.82 to −1.44] vs. −1.24 µm/year [95% CI, −1.34 to−1.07]; $P = 0.005$) and in the inferior sector (−1.41 µm/year [95% CI, −1.56 to−1.34]) vs. 1.10 µm/year [95% CI, −1.24 to−1.04]; $P = 0.01$). No significant differences in rate of change in ONH cube image RNFL thickness were observed between nonprogressing and eyes with progressing glaucoma (all comparisons $P \geq 0.13$).

Discussion

The results from the current sample indicate that OCT imaging measurements using a wide field of view can detect a significant rate of RNFL thinning in healthy eyes, presumably owing to aging, over 28.1 months, whereas measurement from ONH cube-based images cannot. In addition, SWF image measurements can distinguish between the rate of RNFL thinning in eyes with nonprogressing glaucoma and eyes with progressing glaucoma, whereas measurement from ONH cube scans cannot. The first result can aid in discriminating between disease-related change and natural aging-related change, whereas the second result likely can help to discriminate between slow and rapid progressors, which could help to advise level of treatment required to slow or prevent a decrease in visual function and, therefore, quality of life. These results likely are generalizable to high myopia because we included 23.6% highly myopic eyes in our sample. Unfortunately, owing to gaps in imaging owing to COVID longitudinal follow-up was not available in enough myopic eyes to perform meaningful subset analyses in this group.

In summary, when the 3- to 9-mm band RNFL thickness measurements were obtained from the ONH cube scan,

Investigative Ophthalmology & Visual Science

no significant differences in rate of change in RNFL thickness were observed between nonprogressing and eyes with progressing glaucoma (i.e., performance was similar to that of the 3- to 7-mm band suggesting that a wider band on the ONH cube scan does not improve progression detection). In contrast, when we used the 3- to 9-mm measurement band on the larger SWF images to measure RNFL thickness, significant differences between progressing and nonprogressing eyes were observed globally and in the inferior sector ($P \leq 0.01$), suggesting that a wide-field measurement band superimposed on a SWF image can capture progression better than a 3- to 7-mm band superimposed on ONH cube scans.

Other recent studies have demonstrated the superiority of wide-field OCT imaging over standard commercial instrument-based imaging fields for detecting glaucoma in both emmetropic and myopic eyes. For instance, Kim et al.[19,20] compiled a normative database of 220 wide-field swept-source OCT (SS-OCT) images and demonstrated that a normative data based ganglion cell complex deviation map using a 12 × 9 mm^2 wide-field showed improved glaucoma classification performance (based on area under the receiver operating characteristic curve analyses) in early to moderate eyes with glaucoma compared with conventional 6 × 6 mm^2 ganglion cell complex deviation maps. In addition, this group showed a similar improvement for classifying early eyes with glaucoma. Another study by Yu et al.[21] used convolutional neural networks to estimate VF 24-2 MD and VF Index results in healthy, glaucoma suspect (within normal limits Humphrey Field Analyzer results with ocular hypertension, glaucomatous appearance of the ONH or the fellow eye of a glaucoma eye) and eyes with glaucoma using Cirrus OCT measurements from the macula only, ONH only, and macula and ONH combined as network inputs. These authors reported improved convolutional neural network prediction of VF MD (defined as Spearman's rank correlation coefficients and mean absolute estimation error) when macula and ONH measurements were combined, resulting in a larger field of view. More recently, Chiang et al.[22] reported that using a deep learning classifier development approach (convolutional neural network), wide-field OCT images containing information from both the macula and ONH better discriminated between healthy eyes and eyes with glaucoma than ONH scans and macula-centric scans alone with areas under the receiver operating characteristic curve of 0.99 ± 0.01, 0.93 ± 0.06 and 0.91 ± 0.11, respectively. To our knowledge, no studies other than the current one have investigated the effect of field of view on detecting glaucomatous progression in samples composed of patients with and without high myopia.

Regarding myopic eyes, Kim et al.[11] investigated the ability of 12 × 9 mm^2 wide-field SS-OCT thickness measurements and SuperPixel deviation maps compared with 5.2 × 5.2 mm^2 parapapillary and 6 × 6 mm^2 macular thickness and deviation maps for detecting the presence of red-free RNFL evident regional defects (inferotemporal and superotemporal) in myopic eyes with glaucoma and myopic healthy eyes. Subjective assessment of thickness and deviation maps indicated that wide-field imaging improved identification of glaucomatous defects, particularly in the superotemporal macula region. In addition, SS-OCT wide-field imaging resulted in more accurate defect identification than OCT ONH Scan imaging for RNFL thickness maps, ganglion cell–inner plexiform layer (GCIPL) thickness maps and RNFL + GCIPL thickness maps in the inferotemporal region. In the superotemporal region SS-OCT wide-field imaging resulted in more accurate defect identification than OCT ONH cube imaging RNFL thickness maps, RNFL deviation maps, GCIPL thickness maps, GCIPL deviation maps, RNFL + GCIPL thickness maps, and RNFL + GCIPL deviation maps. These results indicate the superiority of wide-field imaging for detecting glaucomatous defects in myopic eyes.

The current study has several limitations. First, obtaining both the ONH and macular scans required to create the stitched SWF image increases imaging time. Second, we may not have included enough eyes with progressing glaucoma or had a long enough follow-up duration to detect significant change over time in RNFL thickness using ONH cube imaging. However, even if significantly declining slopes were observed, the current results suggest strongly that the rates of RNFL thinning would be faster using SWF imaging compared with ONH cube imaging, likely allowing earlier progression detection using wide-field imaging. In addition, we were not able to include enough highly myopic eyes to allow a meaningful comparison between SWR and ONH cube measurements for describing rates of glaucoma-related RNFL thinning in highly myopic eyes vs. non–highly myopic or emmetropic eyes. We are collaborating currently with other laboratories to increase the number of highly myopic eyes with OCT imaging to address these topics in the future. It also is possible that OCT image quality affected differences in RNFL thickness measurement between highly myopic and emmetropic eyes. This situation is unlikely, however, because a post hoc analysis revealed no statistical difference between the signal-to-noise ratio in high myope eyes (26.22 dB [95% CI, 25.19–29.02 dB]) and nonmyopic eyes (27.98 dB [95% CI, 26.32–30.53 dB]) ($P = 0.43$). Because we required repeatable abnormal VF defects to classify eyes as glaucomatous, our sample did not include glaucoma suspects (individuals with suspected glaucomatous optic neuropathy) in the glaucoma group. This choice may have resulted in a greater difference between RNFL thickness measurements at baseline between healthy eyes and eyes with glaucoma shown in Table 2. The fact that we required structural defects to define glaucoma also could have influenced this difference because OCT measurements are not independent of structural defects observed by photographic assessment.

Regarding the possibility that segmentation artifacts often are more common in myopic eyes than emmetropic ones, in a previous study we used SALSA-deep to segment the choroid in myopic eyes very successfully with 379 of 384 scans (98.7%) segmented accurately. The percentage of eyes with choroidal segmentation of good quality exceeded 95% in each of the myopia categories (no myopia, 135 of 139 [97.1%]; mild myopia, 203 of 207 [98.1%]; and high myopia, 41 of 43 [95.4%]).[23] Finally, we have not investigated the repeatability (short-term variability) of SALSA-Deep RNFL and inner limiting membrane measurements used to define global and regional thicknesses of SWF images and ONH cube scans in the current study. It is possible that some random fluctuations in these measurements could occur over time.

In conclusion, the current study showed that mean rate of RNFL thinning was significantly faster in eyes with progressing glaucoma than in eyes with nonprogressing glaucoma using SWF OCT imaging compared with OCT ONH cube imaging over a relatively short follow-up time. These results indicate that using OCT incorporating a large field of view encompassing the macula and optic disc can be effective for monitoring glaucomatous progression in patients with

and without high myopia. Further independent prospective clinical cohort studies with longer follow-up durations are needed to confirm these results.

Acknowledgments

Supported by NIH R01EY011008, NIH R01EY19869, NIH U10EY14267, NIH R01EY027510, NIH R01EY026574, NIH R01EY029058, NIH P30EY022589, Research Fellowship Grant of the German Research Foundation (DFG), and participant retention incentive grants in the form of glaucoma medication at no cost from Novartis/Alcon Laboratories Inc, Allergan, Akorn, and Pfizer Inc. Unrestricted grant from Research to Prevent Blindness, New York, New York, USA.

Disclosure: **C. Bowd**, None; **A. Belghith**, None; **J. Rezapour**, Heidelberg Engineering (F), Santen (F), Bausch & Lomb (F); **J.B. Jonas**, European patent EP 3 271 392, JP 2021-119187, and US 2021 0340237 A1: Agents for use in the therapeutic or prophylactic treatment of myopia or hyperopia (P); **L. Hyman**, None; **R.N. Weinreb**, AbbVie (C), Eyenovia (C), Equinox (C), Nicox (C), Topcon (C), Heidelberg Engineering (R), Carl Zeiss Meditec (R), Centervue (R), Bausch & Lomb (R), Konan Medical (R), Optovue (R), Topcon (R); **L.M. Zangwill**, AbbVie (C), Topcon Medical Systems (C), Carl Zeiss Meditec Inc. (F), Heidelberg Engineering GmbH (F), Optovue Inc. (F), Topcon Medical Systems Inc. (F), ICare Inc. (F), Optomed Inc. (F), AISight Health Inc. (O), AISight Health Inc. (P), Carl Zeiss Meditec (R)

References

1. Bowd C, Hao J, Tavares IM, et al. Bayesian machine learning classifiers for combining structural and functional measurements to classify healthy and glaucomatous eyes. *Invest Ophthalmol Vis Sci*. 2008;49:945–953.
2. Mardin CY, Peters A, Horn F, Junemann AG, Lausen B. Improving glaucoma diagnosis by the combination of perimetry and HRT measurements. *J Glaucoma*. 2006;15:299–305.
3. Mwanza JC, Warren JL, Hochberg JT, Budenz DL, Chang RT, Ramulu PY. Combining frequency doubling technology perimetry and scanning laser polarimetry for glaucoma detection. *J Glaucoma*. 2015;24:561–567.
4. Racette L, Chiou CY, Hao J, et al. Combining functional and structural tests improves the diagnostic accuracy of relevance vector machine classifiers. *J Glaucoma*. 2010;19:167–175.
5. Hood DC, Raza AS, De Moraes CG, et al. Evaluation of a one-page report to aid in detecting glaucomatous damage. *Transl Vis Sci Technol*. 2014;3:8.
6. Raza AS, Zhang X, De Moraes CGV, et al. Improving glaucoma detection using spatially correspondent clusters of damage and by combining standard automated perimetry and optical coherence tomography. *Invest Ophth Vis Sci*. 2014;55:612–624.
7. Shigueoka LS, Vasconcellos JPC, Schimiti RB, et al. Automated algorithms combining structure and function outperform general ophthalmologists in diagnosing glaucoma. *PloS One*. 2018;13:e0207784.
8. Bowd C, Belghith A, Proudfoot JA, et al. Gradient-boosting classifiers combining vessel density and tissue thickness measurements for classifying early to moderate glaucoma. *Am J Ophthalmol*. 2020;217:131–139.
9. Song D, Fu B, Li F, et al. Deep relation transformer for diagnosing glaucoma with optical coherence tomography and visual field function. *IEEE Trans Med Imaging*. 2021;40:2392–2402.
10. Xiong J, Li F, Song D, et al. Multimodal machine learning using visual fields and peripapillary circular OCT scans in detection of glaucomatous optic neuropathy. *Ophthalmology*. 2022;129:171–180.
11. Kim YW, Lee J, Kim JS, Park KH. Diagnostic accuracy of wide-field map from swept-source optical coherence tomography for primary open-angle glaucoma in myopic eyes. *Am J Ophthalmol*. 2020;218:182–191.
12. Bowd C, Belghith A, Rezapour J, et al. Multimodal deep learning classifier for primary open-angle glaucoma diagnosis using wide-field optic nerve head cube scans in eyes with and without high myopia. *J Glaucoma*. 2023;32:841–847.
13. Lee WJ, Na KI, Kim YK, Jeoung JW, Park KH. Diagnostic ability of wide-field retinal nerve fiber layer maps using swept-source optical coherence tomography for detection of preperimetric and early perimetric glaucoma. *J Glaucoma*. 2017;26:577–585.
14. Lee WJ, Oh S, Kim YK, Jeoung JW, Park KH. Comparison of glaucoma-diagnostic ability between wide-field swept-source OCT retinal nerve fiber layer maps and spectral-domain OCT. *Eye (Lond)*. 2018;32:1483–1492.
15. Sample PA, Girkin CA, Zangwill LM, et al. The African Descent and Glaucoma Evaluation Study (ADAGES): design and baseline data. *Arch Ophthalmol*. 2009;127:1136–1145.
16. Jonas JB, Ohno-Matsui K, Panda-Jonas S. Optic nerve head histopathology in high axial myopia. *J Glaucoma*. 2017;26:187–193.
17. Schwarzhans F, Desissaire S, Steiner S, et al. Generating large field of view en-face projection images from intra-acquisition motion compensated volumetric optical coherence tomography data. *Biomed Opt Express*. 2020;11:6881–6904.
18. Gardiner SK, Crabb DP. Examination of different pointwise linear regression methods for determining visual field progression. *Invest Ophthalmol Vis Sci*. 2002;43:1400–1407.
19. Kim H, Park HM, Jeong HC, et al. Wide-field optical coherence tomography deviation map for early glaucoma detection. *Br J Ophthalmol*. 2023;107:49–55.
20. Kim H, Lee JS, Park HM, et al. A wide-field optical coherence tomography normative database considering the fovea-disc relationship for glaucoma detection. *Transl Vis Sci Technol*. 2021;10:7.
21. Yu HH, Maetschke SR, Antony BJ, et al. Estimating global visual field indices in glaucoma by combining macula and optic disc OCT scans using 3-dimensional convolutional neural networks. *Ophthalmol Glaucoma*. 2021;4:102–112.
22. Chiang CYN, Braeu FA, Chuangsuwanich T, et al. Are macula or optic nerve head structures better at diagnosing glaucoma? An answer using artificial intelligence and wide-field optical coherence tomography. *Transl Vis Sci Technol*. 2024;13:5.
23. Rezapour J, Bowd C, Dohleman J, et al. The influence of axial myopia on optic disc characteristics of glaucoma eyes. *Sci Rep*. 2021;11:8854.

Investigative Ophthalmology & Visual Science